Synthetic aperture geoacoustic inversion in the presence of radial velocity and acceleration dynamics

Bien Aik Tan, Peter Gerstoft, Caglar Yardim and William Hodgkiss
Marine Physical Laboratory
Scripps Institution of Oceanography
University of California San Diego
9500 Gilman Drive, La Jolla, California 92093-0238
Email: btan@ucsd.edu, gerstoft@ucsd.edu, cyardim@ucsd.edu and whodgkiss@ucsd.edu

Abstract—A low signal to noise ratio (SNR), single-receiver, broadband, frequency coherent matched-field inversion procedure that exploits coherently repeated transmissions to improve estimation of the geoacoustic parameters recently has been proposed. The long observation time creates a synthetic aperture due to relative source-receiver motion. However, the inversion performance degrades when source/receiver acceleration exists. This paper extends the broadband synthetic aperture geoacoustic inversion to approach cases where the source/receiver radial velocity changes. When this situation exists, it is demonstrated that modeling acceleration is critical for correct inversion. This is done in simulation and real data analysis of low SNR, 100–900 Hz LFM pulses from the Shallow Water 2006 experiment.

I. INTRODUCTION

A single-source and receiver, broadband, frequency coherent matched-field inversion procedure that exploits coherently repeated transmissions to improve estimation of the geoacoustic parameters in low SNR was proposed in [1]. The long observation time creates a synthetic aperture due to relative source-receiver horizontal motion. Though successful, the approach is limited to constant source/receiver radial velocities. Therefore, the assumptions are violated in the region near the closest point of approach (CPA) or when the radial velocities change. Depending on the CPA distance, this CPA region spans from tens to hundreds of meters. This paper extends broadband synthetic aperture geoacoustic inversion to cases where the radial velocity of the source/receiver changes. The method is demonstrated with low SNR, 100–900 Hz LFM data from the Shallow Water 2006 experiment. The improved method is well suited for rapid environment assessment using a horizontally accelerated source and receiver as depicted in Fig. 1. The source or receiver may be towed horizontally by a ship or an autonomous underwater vehicle (AUV). Alternatively, battery powered acoustic source may be dropped onto the ocean bottom to aid AUV-based geoacoustic inversion [2]. The theory of waveguide Doppler and modal propagation is briefly reviewed in Section II, followed by the formulation of the inversion problem. Simulation results are presented in Section III. Section IV presents results from the analysis of experimental data.
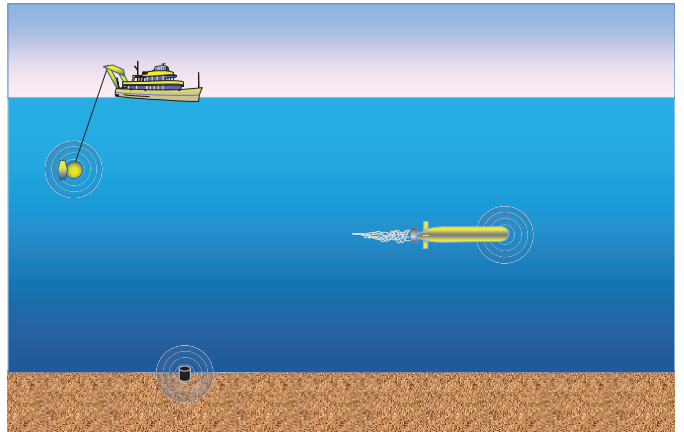

Fig. 1. Illustration of AUV–based geoacoustic inversions

II. THEORY

A. Waveguide Doppler theory model for radial velocity and acceleration dynamics

The waveguide Doppler effect due to source and/or receiver motion on a signal propagating in a range independent waveguide was derived by Schmidt and Kuperman [3][4]. Each horizontal wavenumber or mode will undergo a different Doppler shift. The scenario considered is depicted in Fig. 2. Based on constant source/receiver velocity and depth constraints, the waveguide Doppler shifted field via a normal mode representation is [1]:

$$\psi(\mathbf{r}, z, \omega_r) \approx \frac{ie^{-i\frac{\pi}{4}}}{\sqrt{8\pi}\rho(z_s)} \sum_n S(\omega_s^{(k_n)})$$

$$\Psi_n(z; \omega_r)\Psi_n(z_s; \omega_r)\frac{e^{ik_n r_0}}{\sqrt{k_n r_0}} \quad (1)$$

where

$$\omega_s^{(k_n)} = \omega_r - k_n(v_s - v_r), \quad (2)$$

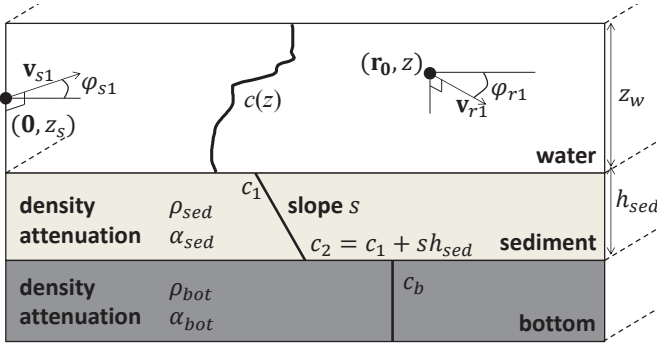$$k_n \approx \frac{k_{rn}}{(1 - \frac{v_r}{u_{rn}})}, \quad (3)$$

Fig. 2. Horizontally stratified ocean with a horizontally moving source and receiver. The source is moving at velocity $\mathbf{v}_s$ and bearing φ_s, while the receiver is moving at velocity $\mathbf{v}_r$ and bearing φ_r. The range origin is defined as the source position at time zero when the source begins transmitting.
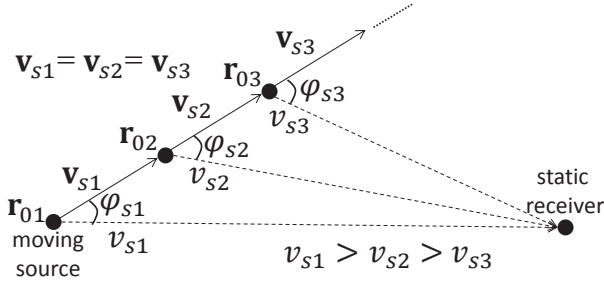

Fig. 3. Top view of a constant velocity source with changing radial velocity due to the geometry of source/receiver position

and

$$S(\omega) = \sum_{p=1}^{P} \exp(i\omega(p-1)T_r)S_c(\omega), \qquad (4)$$

k_n and Ψ_n are the modal wavenumbers and modal functions evaluated at propagation frequencies ω. For numerical efficiency, constructing the field in Eq. (1) is facilitated by some approximations to the propagation modal wavenumbers and functions that are computed instead from ω_r (see Eqs. 1 and 3). $u_{rn} = \frac{d\omega_r}{dk_n(\omega_r)}$ is the nth modal group velocity and $k_{rn} = k_n(\omega_r)$ is the nth modal wavenumber, both evaluated at ω_r. $S(\omega)$ is the source spectrum of P pulses representing the amplitude and phase of the moving point source. T_r is the pulse repetition interval (PRI) and $S_c(\omega)$ is the spectrum of the common or repeated source transmission. r_0 is the source-receiver separation at $t = 0$. In a typical geoacoustic inversion experiment, the source traverses past the receiver as shown in Fig. 3. The source path does not intersect with the receiver for safety reasons. When the source is near the receiver (CPA region), the radial velocity v_s will change even though the source is moving at constant velocity $\mathbf{v_s}$ (see Figs. 3 and 4). The source range near the CPA, where the radial velocity changes significantly, ranges from tens to a few hundreds meters and is a function of CPA distance. In order to perform meaningful inversion near the CPA, acceleration needs to be modeled. However, modeling acceleration is non-trivial as it results in time-dependence in the modal wavenumbers
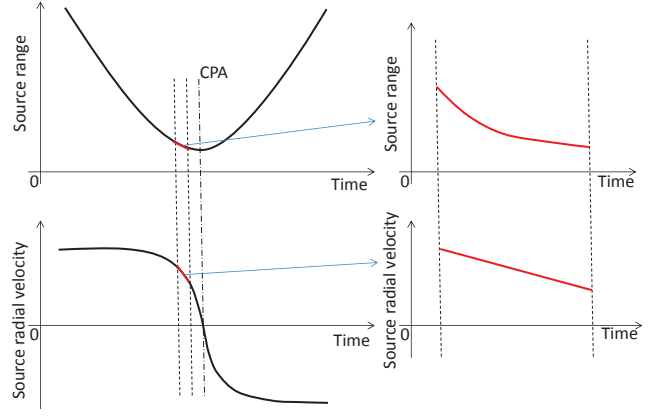

Fig. 4. Source range and radial velocity curves near closest point of approach (CPA)

and functions [5]. An approximate and practical approach is to assume multiple short pulse transmissions, see Eq. (4), where the source/receiver velocities can be assumed piecewise constant but linearly changing from pulse to pulse, as an approximation to a constant acceleration. Therefore, the field can be generated for each pulse and coherently combined for P pulses to form the overall received spectrum. Substituting Eqs. (4) and (2) into Eq. (1) and introducing pulse dependent radial velocities,

$$\psi(\mathbf{r}, z, \omega_r) \approx \frac{ie^{-i\frac{\pi}{4}}}{\sqrt{8\pi}\rho(z_s)} \sum_{p=1}^{P} \sum_{n=1}^{N} \exp(i\omega_r(p-1)T_r)$$

$$\times S_c(\omega_s^{(k_n,p)})\Psi_n(z;\omega_r)\Psi_n(z_s;\omega_r)\frac{e^{ik_{np}r_{0p}}}{\sqrt{k_{np}r_{0p}}} \qquad (5)$$

where

$$\omega_s^{(k_n,p)} = \omega_r - k_{np}(v_{sp} - v_{rp}), \qquad (6)$$

$$k_{np} \approx \frac{k_{rn}}{(1 - \frac{v_{rp}}{u_{rn}})}, \qquad (7)$$

$$v_{sp} = v_{s1} + (p-1)T_r a_s, \qquad (8)$$

$$v_{rp} = v_{r1} + (p-1)T_r a_r, \qquad (9)$$

and

$$r_{0p} = \begin{cases} r_0, & \text{if } p = 1, \\ r_0 + \sum_{j=1}^{p-1} T_r(v_{rj} - v_{sj}), & \text{if } p = 2, \dots, P. \end{cases} \qquad (10)$$

In Eq. (7), the horizontal wavenumber k_{np} is a function of mode and pulse number (pseudo-time dependence). Hence, there are also mode and pulse number dependent frequency mappings when tracing back to ω_s to construct the field at ω_r (see Eq. (6)). The velocities v_{sp} and v_{rp} are modeled to have constant acceleration. Though not done here, it is also possible to model non-constant accelerations using the simple CPA model in Fig. 3 that require the inversion of CPA distance, initial range r_{01} and angles φ_{s1} and φ_{r1}. It is noted that the individual pulses are propagated in the forward model before being coherently combined.

B. Likelihood and cost functions

The broadband data model for frequency-coherent match-field based geoacoustic inversion is [1]

$$\mathbf{y} = \alpha \mathbf{E}(\xi)\mathbf{d}(\mathbf{m}) + \mathbf{w} = \alpha \mathbf{b}(\xi, \mathbf{m}) + \mathbf{w}, \qquad (11)$$

where $\mathbf{y} = [y(\omega_{r1}) \ldots y(\omega_{rJ})]^{\mathrm{T}}$ is the fast Fourier transform (FFT) of the observed time series synchronized to the pulse transmission for J discrete frequencies. α is the complex scalar factor for unknown amplitude scaling and a frequency independent phase shift. $\mathbf{E}(\xi) = \mathrm{diag}[\mathrm{e}^{i\omega_{r1}\xi} \ldots \mathrm{e}^{i\omega_{rJ}\xi}]$ where ξ is the timing error between the source and receiver clocks. The corresponding modeled/replica field $\mathbf{d}(\mathbf{m}) = [\psi(\omega_{r1}, \mathbf{m}) \ldots \psi(\omega_{rJ}, \mathbf{m})]^{\mathrm{T}}$ is generated using Eq. (5) with vector $\mathbf{m}$. $\mathbf{m}$ is a subset of forward model parameters that are being optimized (see Figs. 2 and 3). The distribution of the error vector $\mathbf{w} = [w(\omega_{r1}) \ldots w(\omega_{rJ})]^{\mathrm{T}}$ defines the likelihood function and determines the uncertainty of the model parameters in inverse problems.

Following [1], the optimized inversion parameters obtained via the maximization of the log-likelihood function are

$$\{\xi, \mathbf{m}\}_{ML} = \arg\max_{\xi, \mathbf{m}} \left[\ln L(\xi, \mathbf{m}) \right]$$

$$= \arg\min_{\xi, \mathbf{m}} \left[J \ln \beta(\xi, \mathbf{m}) + J(\ln \pi - \ln J + 1) + \ln |\tilde{\mathbf{C}}_{\mathbf{w}}| \right]$$

$$= \arg\min_{\xi, \mathbf{m}} \left[10 \, \log_{10} \Phi(\xi, \mathbf{m}) \right] \qquad (12)$$

where the cost function

$$\Phi(\xi, \mathbf{m}) = \frac{\beta(\xi, \mathbf{m})}{\mathbf{y}^{\mathrm{H}}\tilde{\mathbf{C}}_{\mathbf{w}}^{-1}\mathbf{y}} = 1 - \frac{|\mathbf{y}^{\mathrm{H}}\tilde{\mathbf{C}}_{\mathbf{w}}^{-1}\mathbf{b}|^2}{\mathbf{y}^{\mathrm{H}}\tilde{\mathbf{C}}_{\mathbf{w}}^{-1}\mathbf{y}\mathbf{b}^{\mathrm{H}}\tilde{\mathbf{C}}_{\mathbf{w}}^{-1}\mathbf{b}} \qquad (13)$$

is the normalized covariance-weighted Bartlett function. In $\mathbf{y}^{\mathrm{H}}\tilde{\mathbf{C}}_{\mathbf{w}}^{-1}\mathbf{b}$, the correlation between the measured and the replica spectrum is inversely weighted by the noise spectrum.

III. SIMULATION

This simulation section shows that taking into consideration acceleration is critical and necessary for correct inversion. The ocean model is illustrated in Fig. 2. The model parameters are tabulated in Table I. Based on the theory, this simulation models a constant velocity moving source that is slowing down radially with respect to the static receiver for $P = 64$ pulses. These range-independent parameters were based on previous SW06 inversion results [6][7][8][9]. The source is a 100–900 Hz LFM pulse with 1 s pulse width and PRI. Colored noise was generated using the measured power spectrum of SW06 noise data. The frequency sampling interval is 5 Hz as done in [1]. The forward model used is KRAKEN [10].

In this simulation, only four representative parameters (z_s, h_{sed}, c_1 and c_{bot}) of various sensitivities were chosen to keep the parameter search space small. The inversions were optimized using a genetic algorithm (GA). The values of the GA parameters are as follows: population size, 16; selection, 0.5; crossover, 0.8; mutation, 0.1; iterations, 8; and parallel populations, 8. Their parameter estimate distributions are plotted in Fig. 5 as histograms. The first Monte Carlo simulation

TABLE I
BASELINE MODEL PARAMETERS.

| Model parameters	value
Source range at $t = 0$, r_0 (m)	600
Source depth, z_{s0} (m)	30
Receiver depth, z_{r0} (m)	45
Source radial velocity, v_{s0} (m/s)	1.9
Receiver radial velocity, v_{r0} (m/s)	0
Source acceleration, a_s (m/s^2)	-0.006
Rcv acceleration, a_r (m/s^2)	0
Water depth, z_w (m)	80
Sediment depth, h_{sed} (m)	22
Sediment density, ρ_{sed} (g/cm^3)	1.8
Sediment attenuation., α_{sed} (dB/λ)	0.2
Sediment top velocity, c_1 (m/s)	1630
Sediment velocity slope, s (1/s)	0
Bottom density, ρ_{bot} (g/cm^3)	2.1
Bottom attenuation., α_{bot} (dB/λ)	0.2
Bottom velocity, c_b (m/s)	1740
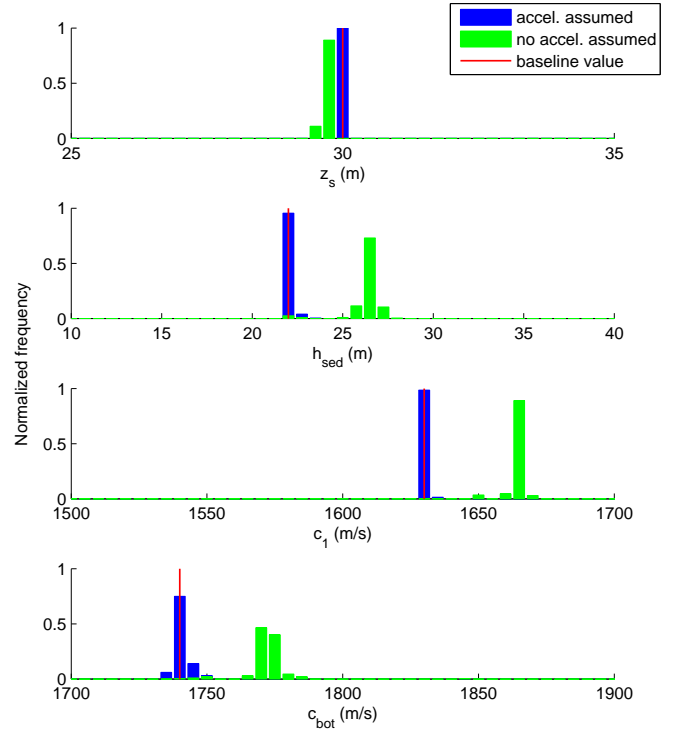
Fig. 5. Histograms of four-parameter inversions for replicas with and without radial acceleration. This Monte Carlo simulation corresponds to 200 noise realizations with SNR fixed at 0 dB and number of LFM pulses $P = 64$.

assumed that the acceleration is known and modeled in the replica. The second Monte Carlo simulation was done where the acceleration is not modeled in the replica. While the first Monte Carlo simulation correctly estimates the parameters, the second Monte Carlo simulation deviates from the correct parameter values.

IV. EXPERIMENTAL DATA ANALYSIS

The SW06 experiment was carried out near the shelf break on the New Jersey continental shelf from July to September
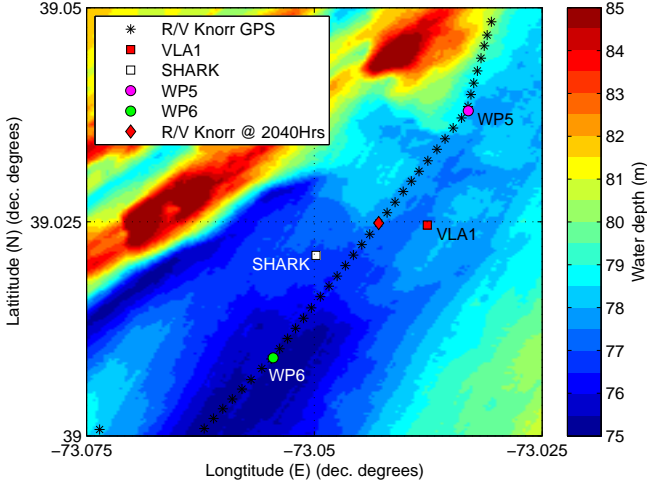
Fig. 6. SW06 experiment site, bathymetry, source and receiver positions on JD238 (26 Aug 2006) 2000–2059 UTC.

Fig. 7. R/V Knorr Telemetry

TABLE II
SW06 DATA INVERSION PARAMETERS SEARCH BOUNDS AND RESULTS FOR $P = 64$.

Model parameters	Lower bound	Upper bound	with a_s opt.	without a_s opt.
Src range at $t = 0$, r_0 (m)	555	625	600	582
Src depth, z_s (m)	27	33	30.3	30.1
Rcv depth, z (m)	41	47	42.8	41.7
Timing error, ξ (msec)	−50	50	−20	−9
Src vel., v_s (m/s)	1.6	2.1	1.9	1.8
Src accel., a_s (m/s$^2 \times 10^{-3}$)	−20	0	−6	n/a
Water depth, z_w (m)	72	82	77.1	76.2
EOF1 coef.	−50	50	36.3	29.5
EOF2 coef.	−25	25	8	10.6
EOF3 coef.	−10	10	3.2	2.7
EOF4 coef.	−10	10	0.9	0.1
EOF5 coef.	−10	10	−1.8	−4.1
EOF6 coef.	−6	2.5	−2.1	−1.3
Sed. dens., ρ_{sed} (g/cm^3)	1	2.5	1.8	1.8
Sed. attn., α_{sed} (dB/λ)	0.001	3	1.4	1.2
Sed. top. vel., c_1 (m/s)	1500	1700	1638	1683
Sed. vel. slope, s (1/s)	−10	10	7.1	0.2
Sed. thickness, h_{sed} (m)	10	40	26.2	23.4
Bot. vel., c_b (m/s)	1700	1900	1805	1797

2006. A data set was chosen with a linearly changing radial velocity moving source and static receiver over a range independent track, see Figs. 6 and 7. The acoustic data is from a 44.6 m deep single receiver, Channel 8 of a vertical line array (VLA1). On JD238 2040 UTC ($t = 0$), 64 LFM pulse (100–900 Hz) transmissions were made from a 30 m deep J-15 source towed by the R/V Knorr at an initial radial velocity of 1.6 m/s and acceleration of −0.006 m/s^2 with respect to VLA1. The LFM pulse width is 1 s and is repeated every second. Correspondingly, the towed source displacement with respect to VLA1 or synthetic aperture is (1.6 m/s − 64/2 × (0.006 m/s^2))× 64 s = 90 m long. The R/V Knorr GPS range to VLA1 was 525 m with a CPA distance of 410 m and the source is known to be trailing 115 m behind the ship's GPS mast. Based on the ship and VLA1 positions, the search bounds for the actual source to VLA1 distance at $t = 0$ is estimated to be 555–625 m. Due to the lack of CTD measurements during this period and location, sound speed profile inversion was included using empirical orthogonal functions [11][6][7] (EOFs) based on sound speed profiles (SSPs) derived from thermistors along the SHARK array (see Fig. 6) [1].

A. Matched-field geoacoustic inversion

The inversion search bounds were set for the forward model depicted in Fig. 2 based on the background information at the experiment site. These are tabulated in Table II. The 19-parameter matched field inversion algorithm used here is based on a multi-step approach [1]. GA performed the minimization of the cost function Eq. (12). The values of the GA parameters are as follows: population size 512, selection 0.5, crossover 0.8, mutation 0.02, iterations 32 and parallel populations 12. Pre-processing of the single receiver data include LFM pulse matched filtering for coarse synchronization and the fast Fourier Transform (FFT) of the 64 s data is carried out to obtain the measured field in the frequency domain.
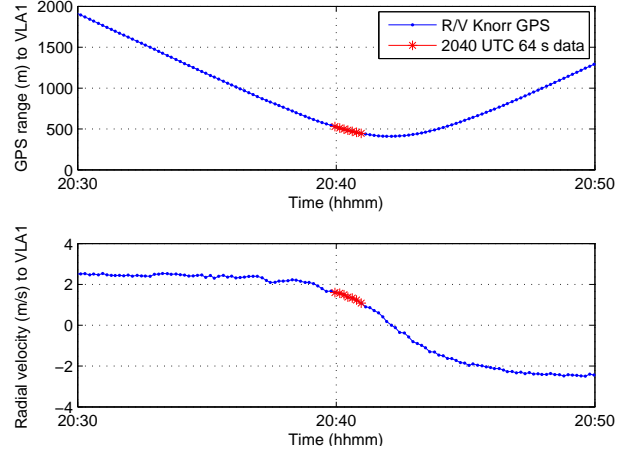
Table II tabulates the inversion results using the waveguide Doppler model with and without acceleration modeled for the 64 LFM pulses. For the waveguide Doppler model with acceleration results, the estimated sediment thickness, velocity and density are consistent with other published results [6][7][8][9] at the VLA1 site.

Scatter plots can be used to compare sensitivities and estimation uncertainties between the two inversions. Fig. 8 shows the scatter plots for selected parameters of the cost function values plotted for waveguide Doppler with and without acceleration model evaluated in GA ($P = 64$ pulses). The scatter plots provide information about the real sensitivities of the parameters by observing the envelopes of the scatter plots. A lower and sharper minimum usually indicates lower estimation uncertainty. The inversion is also sensitive to source radial velocity and acceleration (2nd row of Fig. 8(a)). However, the inversion's 1.9 m/s source initial velocity result does not
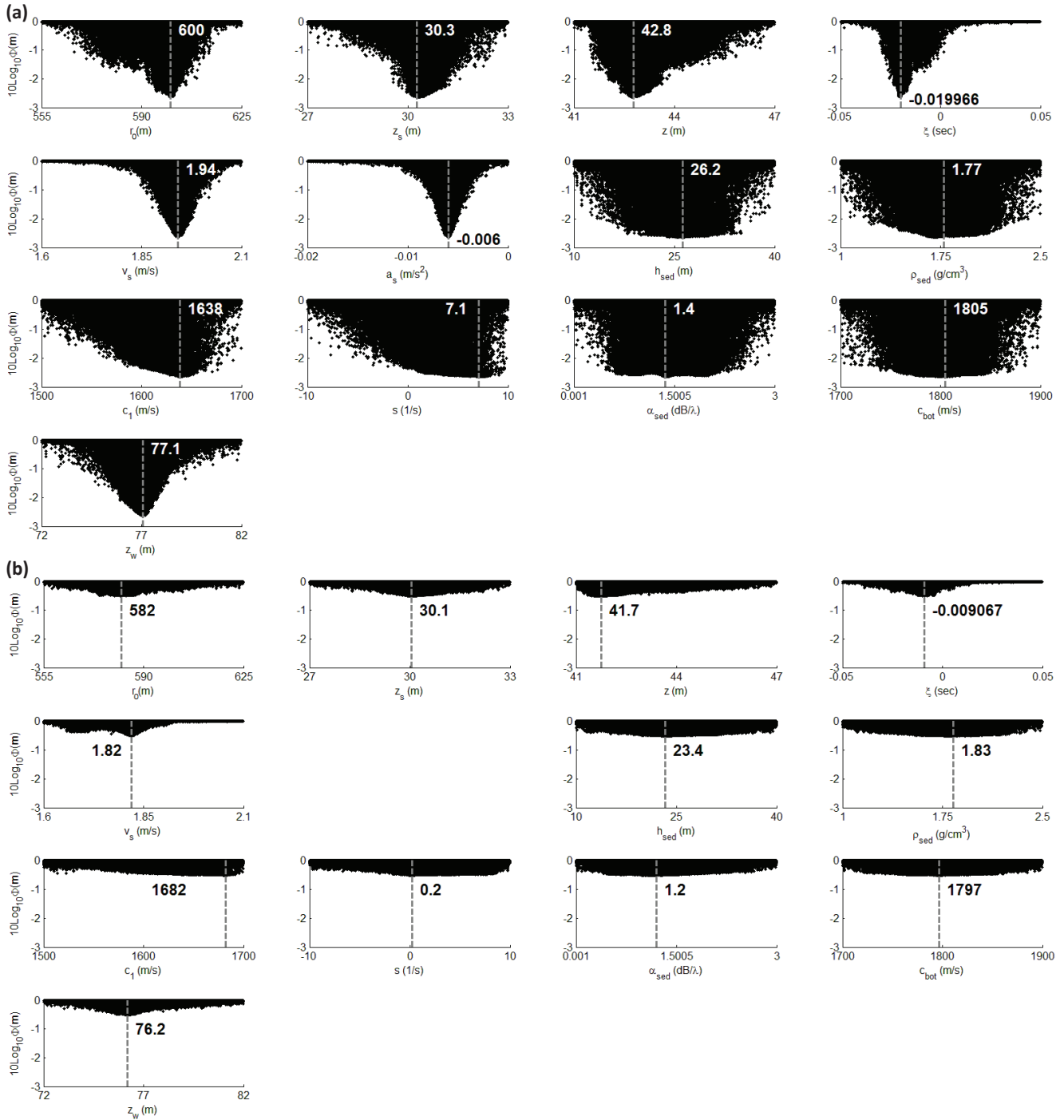
Fig. 8. SW06 64 s data inversion scatter plots for $P = 64$ pulses using waveguide Doppler model (a) with acceleration and (b) without acceleration. The vertical dashed line shows the final inversion results with SNR $\approx$ 0 dB.
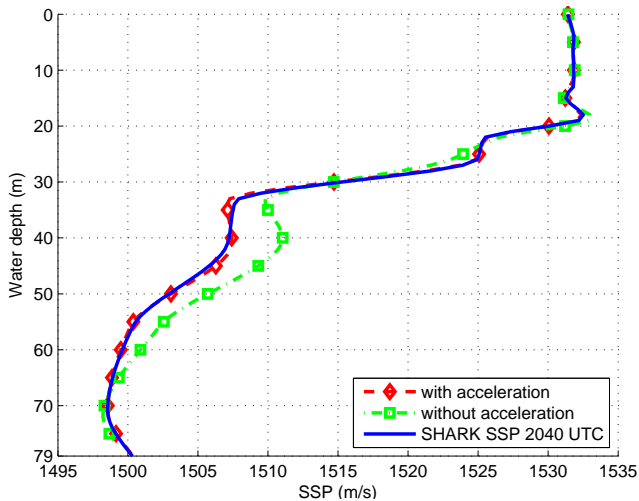
Fig. 9. SSP inversion results using SW06 experimental data and $P = 64$ pulses using waveguide Doppler with acceleration and without acceleration.

agree with the 1.6 m/s velocity estimated from the GPS ship track. The waveguide Doppler with acceleration scatter plots also show a lower minimum cost value indicating that it is a better model than the model without acceleration. Without the acceleration model, there are different velocity minima for individual pulses as their source radial velocity ranges from 1.9 to 1.6 m/s (see Fig. 8(b) for v_s).

Fig. 9 shows the estimated water column SSPs using the waveguide Doppler model with and without acceleration. The EOFs have allowed the inversion to optimize the best range-independent SSP which is also the one using the waveguide Doppler with acceleration model. The inverted SSP is very similar to the SSP measured by the SHARK thermistor array at 2040 UTC.

V. Conclusions

This paper extends broadband synthetic aperture geoacoustic inversion to cases where the source/receiver radial velocity changes. The improved method is well suited for a horizontally accelerated source and receiver. Through simulation and real data analysis of the Shallow Water 2006 experiment, it is demonstrated that acceleration should be modeled appropriately in the replica for correct inversion.

Acknowledgment

References

[1] B. A. Tan, P. Gerstoft, C. Yardim, and W. S. Hodgkiss, "Broadband synthetic aperture geoacoustic inversion," *J. Acoust. Soc. Am.*, vol. 134, no. 1, pp. 312–322, 2013.

[2] D. P. Massa and J. I. Arvelo, "A wideband moving coil electrodynamic transducer system for autonomous underwater vehicle-based geoacoustic inversion," *J. Acoust. Soc. Am.*, vol. 132, no. 3, pp. 1920–1920, 2012.

[3] H. Schmidt and W. A. Kuperman, "Spectral and modal representations of the Doppler-shifted field in ocean waveguides," *J. Acoust. Soc. Am.*, vol. 96, no. 1, pp. 386–395, 1994.

[4] F. B. Jensen, W. A. Kuperman, M. B. Porter, and H. Schmidt, *Computational Ocean Acoustic*, 2nd ed., ser. Modern Acoustics and Signal Processing.   New York: Springer, 2011, pp. 623–629.

[5] S. C. Walker, P. Roux, and W. A. Kuperman, "Modal Doppler theory of an arbitrarily accelerating continuous-wave source applied to mode extraction in the oceanic waveguide," *J. Acoust. Soc. Am.*, vol. 122, no. 3, pp. 1426–1439, 2007.

[6] C.-F. Huang, P. Gerstoft, and W. S. Hodgkiss, "Effect of ocean sound speed uncertainty on matched-field geoacoustic inversion," *J. Acoust. Soc. Am.*, vol. 123, no. 6, pp. EL162–EL168, 2008.

[7] Y.-M. Jiang and N. R. Chapman, "Bayesian geoacoustic inversion in a dynamic shallow water environment," *J. Acoust. Soc. Am.*, vol. 123, no. 6, pp. EL155–EL161, 2008.

[8] J. W. Choi, P. H. Dahl, and J. A. Goff, "Observations of the R reflector and sediment interface reflection at the shallow water '06 central site," *J. Acoust. Soc. Am.*, vol. 124, no. 3, pp. EL128–EL134, 2008.

[9] C. Park, W. Seong, P. Gerstoft, and W. S. Hodgkiss, "Geoacoustic inversion using backpropagation," *IEEE J Ocean. Eng.*, vol. 35, no. 4, pp. 722–731, 2010.

[10] M. B. Porter, "The KRAKEN normal mode program," SACLANTCEN Memo. SM-245 (SACLANT Undersea Research Centre, La Spezia, Italy, 1991, chap. 2.

[11] P. Gerstoft and D. F. Gingras, "Parameter estimation using multifrequency range-dependent acoustic data in shallow water," *J. Acoust. Soc. Am.*, vol. 99, no. 5, pp. 2839–2850, 1996.